Journal of Crystal Growth 323 (2011) 446–449

Contents lists available at ScienceDirect

Journal of Crystal Growth

journal homepage: www.elsevier.com/locate/jcrysgro

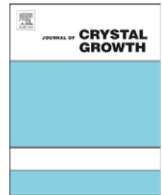

MBE growth of low threshold GaSb-based lasers with emission wavelengths in the range of 2.5–2.7 μm

Kristijonas Vizbaras *, Alexander Bachmann, Shamsul Arafin, Kai Saller, Stefan Sprengel, Gerhard Boehm, Ralf Meyer, Markus-Christian Amann

Walter Schottky Institut, Technische Universität München, Am Coulombwall 3, 85748 Garching, Germany

ARTICLE INFO

Available online 2 December 2010

Keywords:
A3. Molecular beam epitaxy
B1. Antimonides
B2. Semiconducting quaternary alloys
B3. Infrared devices
B3. Laser diodes

ABSTRACT

In this work, we present our approach towards the growth of active regions and cladding layers for GaSb based record low-threshold lasers emitting in the range of 2.5–2.7 μm. First, a study on Sb incorporation in the AlGaAsSb cladding layers and GaInAsSb QWs is presented as a function of growth temperature. A linear decrease in Sb incorporation was observed for both cases. Second, a choice of well-barrier material is presented. Here, the best results have been achieved with a GaSb/GaInAsSb combination, yielding a low-temperature (20 K) photoluminescence (PL) response with a very narrow full-width at half-maximum (FWHM) of 4.5 meV. The latter is followed by an investigation of active region degradation with increased annealing temperatures. The rapid degradation has been confirmed by PL and X-ray diffraction studies. Finally, device results are presented. Lasers show ultra-low CW threshold current densities (44 A/cm^2 at $L\rightarrow\infty$), in the wavelength range of 2.5–2.7 μm.

© 2010 Elsevier B.V. All rights reserved.

1. Introduction

Lasers emitting in the mid-infrared wavelength range above 2 μm are attractive light sources for trace-gas sensing systems based on tunable diode laser absorption spectroscopy (TDLAS) [1]. Many important industrial gases show strong absorption lines in the spectral range between 2 and 3 μm, which are accessible with GaSb-based devices, making them the most promising candidates for gas sensing applications. InP-based devices are limited to an emission wavelength of 2.3 μm [2]; therefore, for longer wavelengths, GaSb-based devices have to be used. Here, in order to reach longer wavelengths, one has to increase the amount of indium in the quaternary GaInAsSb quantum well (QW) material. This brings the alloy deeper into the miscibility gap [3], making growth more complicated. Moreover, one has to grow highly strained active regions to have enhanced gain [4]. In this work, we present our approach towards the growth of active regions and cladding layers for GaSb based record low-threshold lasers emitting in the range of 2.5–2.7 μm [5]. First, a study on Sb incorporation in the AlGaAsSb cladding layers and GaInAsSb QWs is presented as a function of growth temperature. A linear decrease in Sb incorporation was observed in both cases. Second, a choice of well-barrier material is presented. Here, the best results have been achieved with a GaSb/GaInAsSb combination, yielding a low-temperature (20 K) photoluminescence (PL) response with a very narrow full-width at half-maximum (FWHM) of 4.5 meV. The latter is followed by an investigation of active region degradation with increased annealing temperatures. The rapid degradation has been confirmed by PL and X-ray diffraction studies. Finally, device results are presented. Lasers show ultra-low CW threshold current densities (44 A/cm^2 at $L\rightarrow\infty$), in the wavelength range of 2.5–2.7 μm.

2. Epitaxy

MBE growth of GaSb-based lasers typically involves growth of alloys that have two group-V components. This requires more sophisticated growth calibration, because group-V incorporation coefficients are not the same for different alloys and also depend on growth conditions, such as temperature, V/III ratio, growth rate, strain and material composition [6–9]. In our work we define the Sb incorporation coefficient in the following manner:

$$C=\frac{\Phi_{As}}{\Phi_{Sb}}\left(\frac{x_{Sb}}{1-x_{Sb}}\right) \quad (1)$$

Here Φ_{As} and Φ_{Sb} are arsenic and antimony fluxes, respectively, measured with a flux filament gauge and x_{Sb} is the atomic percentage of antimony in the alloy, determined from X-ray diffraction (XRD) simulation. In this manner one is able to choose the required arsenic overpressure for a desired material composition at a fixed temperature, strain and V/III ratio. For epitaxial growth of devices a Varian Mod Gen-II MBE system with solid sources for group-III elements and valved cracker-cells for arsenic

* Corresponding author.
E-mail address: Kristijonas.Vizbaras@wsi.tum.de (K. Vizbaras).

0022-0248/$ - see front matter © 2010 Elsevier B.V. All rights reserved.
doi:10.1016/j.jcrysgro.2010.11.139

and antimony was used. Te and Si were used as *n* and *p*-type dopants, respectively.

Edge-emitting laser growth typically starts with the cladding and waveguide layers, which are thick lattice-matched AlGaAsSb layers. In this step, precise knowledge of Sb incorporation coefficient is required, due to the fact that the active region is typically grown directly after the quaternary layers mentioned above. These are typically 2.5 μm thick, so that very little lattice mismatch can be tolerated. The partial relaxation of such layers would lead to roughness, which deteriorates the optical quality and result in a bad device performance.

Incorporation of Sb in AlGaAsSb, lattice matched to GaSb, was investigated in the temperature range from 470 to 510 °C. The temperature was measured by means of optical pyrometry, calibrated to the GaSb oxide desorption temperature of 540 °C. A beam equivalent pressure (BEP) V/III ratio of 1.5 was found to result in the best surface morphology, indicated by the absence of scattered light from the optical microscope. This ratio was kept constant during all growth experiments. The composition of the quaternary layers was determined by means of XRD rocking curve simulations. Here, group-III rates were calibrated prior to the quaternary layer growth by growing an AlSb/GaSb superlattice (SL) with 150 nm thick bulk AlGaSb on top and simulating the measured XRD rocking curve. Since the sticking coefficients of group-III elements in the investigated temperature range were equal to 1 [10,11], Ga and Al concentrations were considered to be known in the simulation, while strain was simulated as a result of the As/Sb ratio. Such an assumption is reasonable, because the error in determining group-III rates is typically in the 1–2% range, which would result in changes of strain of the order of 0.006%. It was found that antimony incorporation strongly increases with decreasing growth temperature (Fig. 1), which can be explained by the slowing down of As/Sb exchange reaction at the growth surface [6]. Under the investigated growth conditions, the Sb incorporation factor exhibited a linear dependence on temperature, making it easy to adjust arsenic overpressure for the required composition. In addition, it was found to be independent of aluminium concentration in the quaternary layer across the entire investigated range (10–50%), which is in good agreement with the observations by Selvig et al. [7].

The optimization of epitaxial growth for active regions consists of several steps: (1) The Sb incorporation factor for given growth conditions has to be determined, (2) a barrier material has to be chosen and (3) optimum growth temperature for the layers above the active region has to be chosen.

The determination of the Sb incorporation coefficient was carried out in the same manner as for the AlGaAsSb layers. MQW GaInAsSb/GaSb structures were used for composition determination from HRXRD rocking curve simulation. Since the barriers are lattice matched, strain is governed by the As/Sb ratio in the QWs, as the Ga and In concentrations are known (within 2% error rate) from group-III growth rate calibration, which was done prior to the active structure growth. Such an assumption allows one to estimate the Sb incorporation coefficient within 6% error range. Here, we have neglected the intermixing of atoms between well and barrier, because growth was terminated right after the MQW structure and, therefore, it was not exposed to any excess annealing that could lead to inter-diffusion. We have investigated the incorporation coefficient as a function of growth temperature at a fixed growth rate, strain (adjusted for enhanced gain) and V/III ratio of 2. Results are depicted in Fig. 1. The Sb incorporation factor was found to increase linearly with decreasing temperature, due to reduced As/Sb exchange, however, at a lower rate than in AlGaAsSb (Fig. 1). This could be explained by the stronger Al-V bonds [14], which require more energy to brake and, therefore, the As/Sb exchange reduces faster with decreasing temperature.

The second part of the active region design consists of a proper choice of barrier material. This can be either AlGaAsSb or GaSb. AlGaAsSb offers the possibility of strain compensation and better hole confinement, but has very high conduction band offsets, which will affect the filling of the wells. Additionally, quaternary AlGaAsSb has higher heat resistivity, which strongly decreases with increasing Al content [12]. For example, the heat resistivity of GaSb is around 3 cmK/W, a value more than 4 times smaller than that of $Al_{0.5}Ga_{0.5}As_{0.04}Sb_{0.96}$. Moreover, GaSb barriers provide better filling of the QWs due to lower conduction band offsets and are easy to grow. However, hole confinement gets critical for active regions designed for longer emission wavelengths and, above 3 μm, usage of aluminium containing layers is unavoidable.

The active regions were grown at 470 °C, which was found to result in a maximum PL intensity. We have also found that the barrier material has a strong influence on the optical properties of the QWs. With increasing Al content in the barrier, the full-width at half-maximum (FWHM) of the low temperature photoluminescence (PL) response increases nearly 3 times for $Al_{0.33}Ga_{0.67}As_{0.03}Sb_{0.97}$ barriers (Fig. 2), when compared to QWs with GaSb barriers.

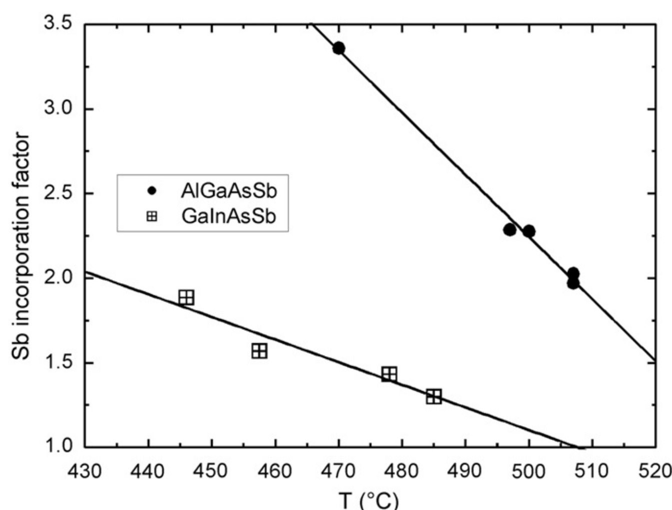

Fig. 1. Sb incorporation factor as a function of growth temperature for AlGaAsSb lattice matched to GaSb (full circles) and for compressively strained (1.7%) GaInAsSb.

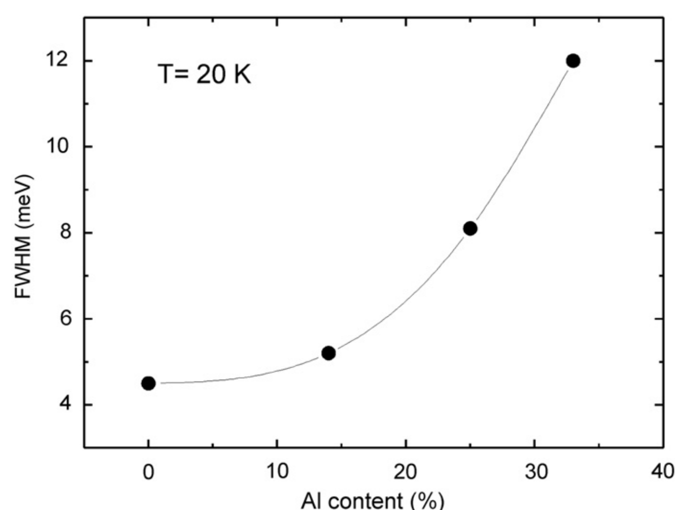

Fig. 2. FWHM of PL response of 1.6% compressively strained QW at 20 K as a function of aluminum content in the AlGaAsSb barrier material. 0% stands for GaSb barriers.

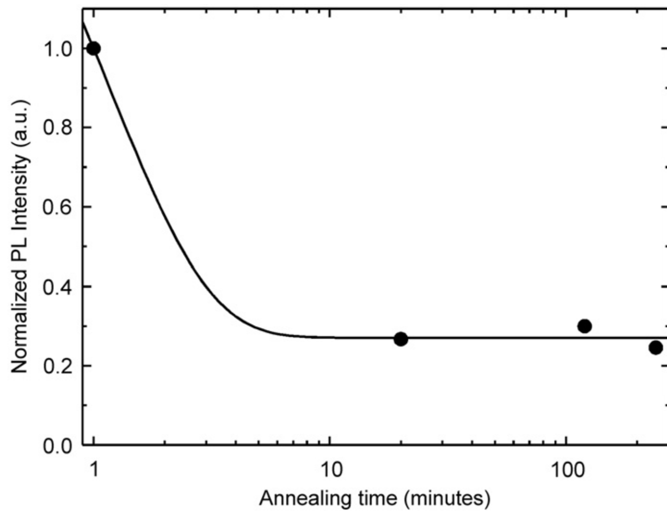

Fig. 3. Normalized PL intensity at 300 K as a function of annealing time at 500 °C for $Ga_{0.67}InAs_{0.13}Sb/Al_{0.33}GaAs_{0.03}Sb$ QWs. The solid line has no physical meaning and is just a guide to the eye.

We attribute such behaviour to alloy broadening [13] and to the possibility of quinternary AlGaInAsSb interface creation between the well and the barrier, since no special shutter sequence was introduced for specific interface formation. Here, interface irregularities and defects might be causing the broadening of PL response. To summarize, the best optical properties for emission around 2.7 μm have been achieved with $Ga_{0.57}In_{0.43}As_{0.15}Sb_{0.85}$ quantum wells embedded in GaSb barriers. PL response with a FWHM of 4.5 meV at 20 K has been measured.

Finally, the optimum growth temperature of layers above the active region has been investigated. We have found that active regions are prone to rapid degradation with increased annealing temperatures. PL intensity drops rapidly with annealing (Fig. 3), independent of the barrier material used. Additionally, XRD scans of the as-grown and annealed samples, with GaSb barriers, indicate that crystal degradation starts immediately when annealed at 500 °C. Already after 5 min of annealing, a change in the rocking curve can be observed and satellite peaks start broadening and smearing out (Fig. 4). This indicates that some roughening or intermixing is happening at the interface. Similar annealing effects are described by Turner et al. [14]. Such crystalline degradation goes hand in hand with deterioration of optical properties—PL intensity drops rapidly and emission wavelength shifts towards higher energies, supporting the assumption of intermixing, a known phenomenon in GaSb-based material systems [15–17]. In contrast to the active regions with GaSb barriers, active regions with AlGaAsSb barriers in a wide range of Al concentrations (15–50%) do not show such crystalline degradation and the XRD rocking curve remains unchanged even when annealed for 2 h at 500 °C (Fig. 4). The reason for such behaviour could be the reduction of the intermixing site density by adding Al, as binding energies of AlAs and AlSb are reasonably higher than the ones for GaSb, InSb, GaAs and InAs [18] and the latter binaries are expected to participate more strongly in intermixing processes. Despite the fact that roughening of interfaces seemed to be suppressed in Al-containing barriers, degradation of optical quality was similar to that of the active regions with GaSb barriers.

Therefore, for laser growth, the approach of active regions with GaSb barriers was chosen, while trying to grow the upper cladding layers at the same temperature as the active region (470 °C) to avoid unwanted in-situ annealing effects. The cladding material was chosen to be $Al_{0.5}Ga_{0.5}As_{0.04}Sb_{0.96}$, so that no degradation due to oxidation would occur during processing. For the waveguide

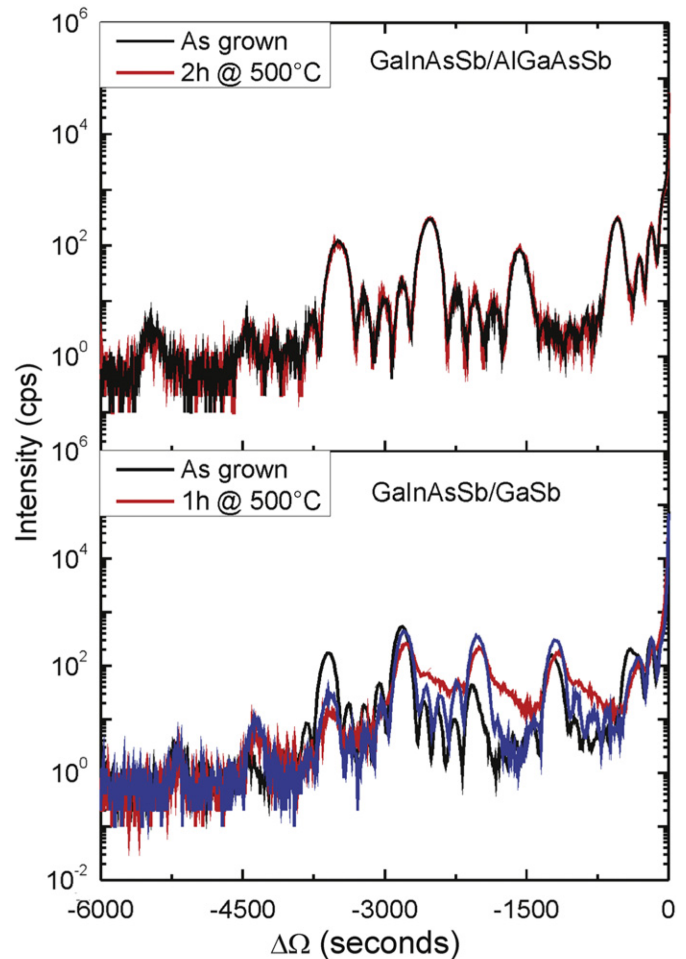

Fig. 4. XRD (0 0 4) rocking curve of 5 compressively strained GaInAsSb QWs embedded in AlGaAsSb barriers (top) and GaSb barriers (bottom). The effect of temperature induced degradation on crystalline quality of the active region is shown.

$Al_{0.1}Ga_{0.9}As_{0.01}Sb_{0.99}$ was chosen. Both waveguide and cladding, provided a sufficient transversal optical confinement factor (1–2% per QW) to ensure laser operation. For the active region, highly compressively strained $Ga_{0.57}In_{0.43}As_{0.15}Sb_{0.85}$ QWs embedded in GaSb barriers were chosen. The wavelength range from 2.5 to 2.7 μm was covered by changing the width of the wells from 10 to 20 nm, respectively.

3. Fabrication

The grown devices were processed as ridge-waveguide lasers, with lithographically defined ridges, ranging from 60 to 5 μm in width. Processed devices were cleaved into laser bars of lengths ranging from 3 mm to 300 μm and were mounted epi-side up on the copper heatsinks. Mirror facets were left as cleaved—no coatings were applied.

4. Device results

Despite the previously mentioned growth difficulties, the grown devices exhibited continuous-wave (CW) operation with record low-threshold current densities in the wavelength range of 2.5–2.7 μm (Fig. 5), at 15 °C [5]. Single quantum well (SQW) devices emitting at 2.53 μm had an extrapolated CW threshold current

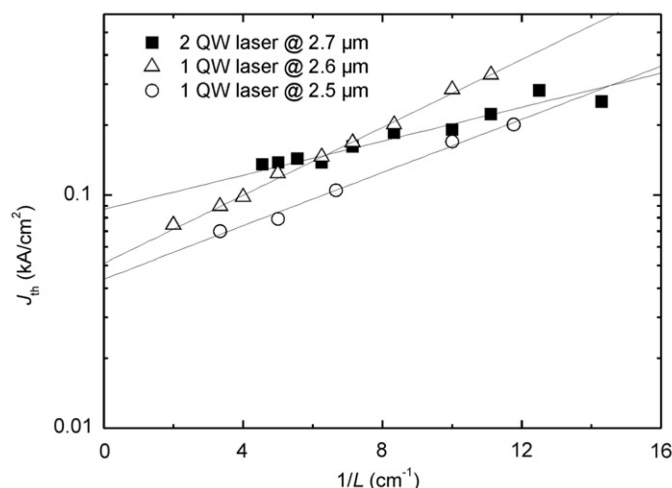

Fig. 5. Threshold current density for devices with 60 µm wide ridges, under CW operation, as a function of inverse cavity length at 288 K.

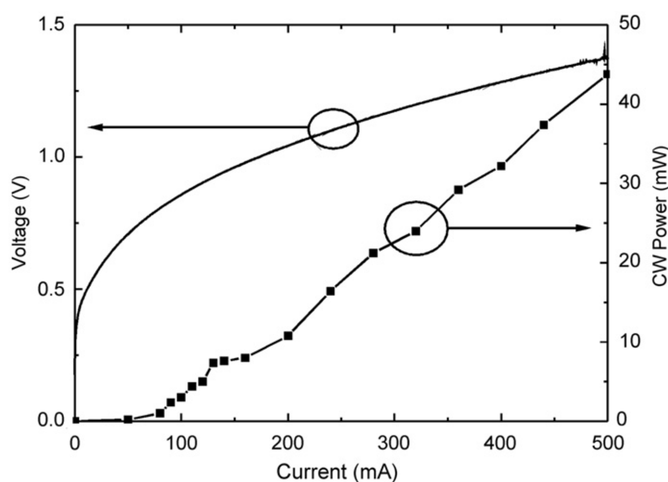

Fig. 6. Power–current and voltage–current characteristics of a 1.2 mm long 2QW laser with 30 µm wide ridge, emitting at 2.72 µm, at 288 K. The power is given for both facets.

density of 44 A/cm^2 for infinite length. The measured CW threshold current density was 70 A/cm^2 for a 3 mm long device. Lasers emitting at 2.65 µm had an extrapolated CW threshold current density of 50 A/cm^2 and a measured one of 70 A/cm^2 for 3 mm long devices. 2 QW devices, emitting at 2.72 µm, exhibited an extrapolated CW threshold current density of 87 A/cm^2 and had a measured value of 136 A/cm^2 for 2.2 mm long devices (Fig. 5). The extracted threshold currents include the current broadening effect, which was evaluated from threshold current dependency on ridge width. The extracted value was found to be 4.2 µm for both sides. The lasers are operated in CW up to 55 °C. Power–current and voltage–current characteristics for a 2 QW device, emitting at 2.72 µm are shown in Fig. 6. A maximum CW output power of 44 mW per facet was achieved and is limited by the current source. Internal losses of 3 cm^{-1} were extracted from the dependence of differential efficiency on cavity length. Such a low value is in good agreement with the excellent device performance. Characteristic temperatures were found to be in the range of 65–42 K. The higher value was found for devices emitting at 2.72 µm and the lower one for devices emitting at 2.5 µm. The exact reason for such behaviour is not fully understood, but can be partially explained by increased carrier leakage due to lower confinement in thinner wells.

5. Conclusion

Excellent device performance and record-low threshold current densities in the wavelength region of 2.5–2.7 µm have been achieved. Such a device performance is the direct evidence of very good epitaxial growth quality and the potential of the material system, which can be applied to produce efficient, single-mode light sources for trace-gas sensing, such as vertical-cavity surface-emitting lasers (VCSELs) and distributed feedback lasers (DFBs).

6. Future outlook

In order to cover a spectral range of gas absorption lines up to 3 µm, further improvement of active region growth is necessary. GaSb barriers cannot be used anymore due to type-II band alignment and active regions with quaternary AlGaAsSb or even quinternary AlGaInAsSb have to be considered.

Acknowledgment

This work has been supported by the European Union via NEMIS project (Contract no. FP6-2005-IST-5-031845).

References

[1] A. Vicet, D.A. Yarekha, A. Pérona, Y. Rouillard, S. Gaillard, A.N. Baranov, Spectrochim. Acta, Part A 58 (2002) 2405–2412.
[2] M. Ortsiefer, G. Boehm, M. Grau, K. Windhorn, E. Ronneberg, J. Rosskopf, R. Shau, O. Dier, M.–C. Amann, Electron. Lett. 42 (11) (2006) 640–641.
[3] V. Sorokin, S. Sorokin, A. Semenov, B. Meltser, S. Ivanov, J. Cryst. Growth 216 (2000) 97–103.
[4] A.R. Adams, Electron. Lett. 22 (1986) 249.
[5] K. Kashani-Shirazi, K. Vizbaras, A. Bachmann, S. Arafin, M.-C. Amann, IEEE Photon. Technol. Lett. 21 (2009) 1106–1108.
[6] Q. Xie, J.E. Van Nostrand, J.L. Brown, C.E. Stutz, J. Appl. Phys. 86 (1) (1999) 329–336.
[7] E. Selvig, B.O. Fimland, T. Skauli, R. Haakenaasen, J. Cryst. Growth 227-228 (2001) 562–565.
[8] G. Almuneau, E. Hall, S. Mathis, L.A. Coldren, J. Cryst. Growth 208 (2000) 113–116.
[9] S. Simanowski, M. Walter, J. Schmitz, R. Kiefer, N. Herres, F. Fuchs, M. Maier, C. Mermelstein, J. Wagner, G. Weimann, J. Cryst. Growth 201 (1999) 849–853.
[10] J.M. Van Hove, P.I. Cohen, Appl. Phys. Lett. 47 (1985) 726–728.
[11] J.-P. Reithmaier, H. Riechert, H. Schlötterer, G. Weimann, J. Cryst. Growth 111 (1991) 407–412.
[12] A. Bochkarev, B.A. Drakin, P. Sverdlov, Electron. Lett. 26 (7) (1990) 418–419.
[13] E.F. Schubert, E.O. Göbel, Y. Horikoshi, K. Ploog, H.J. Queisser, Phys. Rev. B 30 (2) (1984) 813–820.
[14] M.O. Manasreh, G.W. Turner, H.K. Choi, Optoelectron. Prop. Semicond. Superlattices 3 (1997) 369–431.
[15] Y. Wang, H.S. Djie, B.S. Ooi, J. Appl. Phys. 98 (2005) 073508.
[16] Y. Wang, H.S. Djie, B.S. Ooi, P. Rotella, P. Dowd, V. Aimez, Y. Cao, Y.H. Zhang, Thin Solid Films 515 (2007) 4352–4355.
[17] O. Dier, S. Dachs, M. Grau, C. Lin, C. Lauer, M.-C. Amann, Appl. Phys. Lett. 86 (15) (2005) 151120.
[18] C.Y. Yeh, A.B. Chen, Phys. Rev. B 43 (11) (1991) 9138–9151.